A method for reconstructing the solar wind stream structure beyond Earth's orbit

M.M. Kalinichenko[1], M.R. Olyak[1], O.O. Konovalenko[1], A.I. Brazhenko[2],
O.L. Ivantishin[3], O.O. Lytvynenko[1] , I.M. Bubnov[1], S.M. Yerin[1] , N.V. Kuhai[4], O.I. Romanchuk[5]

[1]Radio Astronomy institute of NAS of Ukraine, Kharkiv, Ukraine
kalinich@ri.kharkov.ua

[2] Gravimetrical observatory of Geophysical institute of NAS of Ukraine, Poltava, Ukraine

[3] Institute of Physics and Mechanics of NAS of Ukraine, Lviv, Ukraine

[4] National Pedagogical Dragomanov University, Kyiv, Ukraine

[5] Hlukhiv national pedagogical university, Hlukhiv, Ukraine

Plan of report

- Stream structure of the solar wind.

- Observations of the interplanetary scintillations (IPS) at decameter wavelengths.

- Method for reconstructing the solar wind stream structure.

- Results of data processing and modeling.

Coronal and Solar Wind Stream Structure

The corona is highly non-uniform. It is thus not surprising that the solar wind also is highly structured.

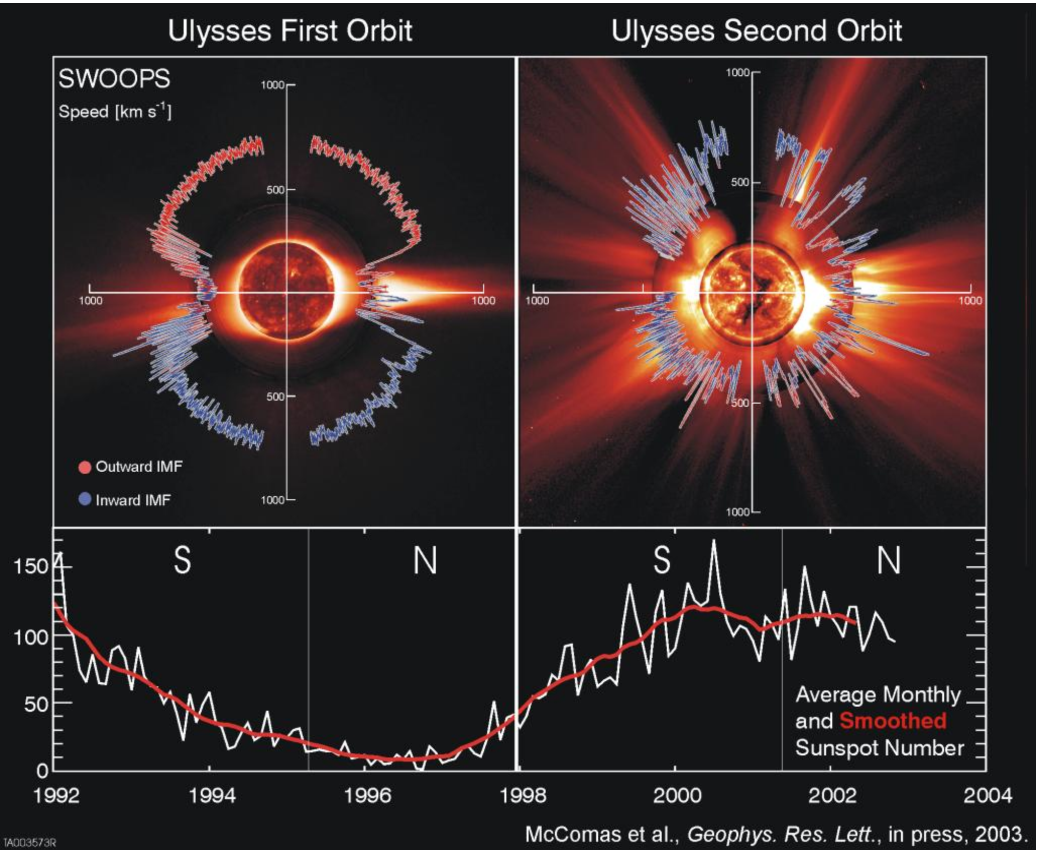

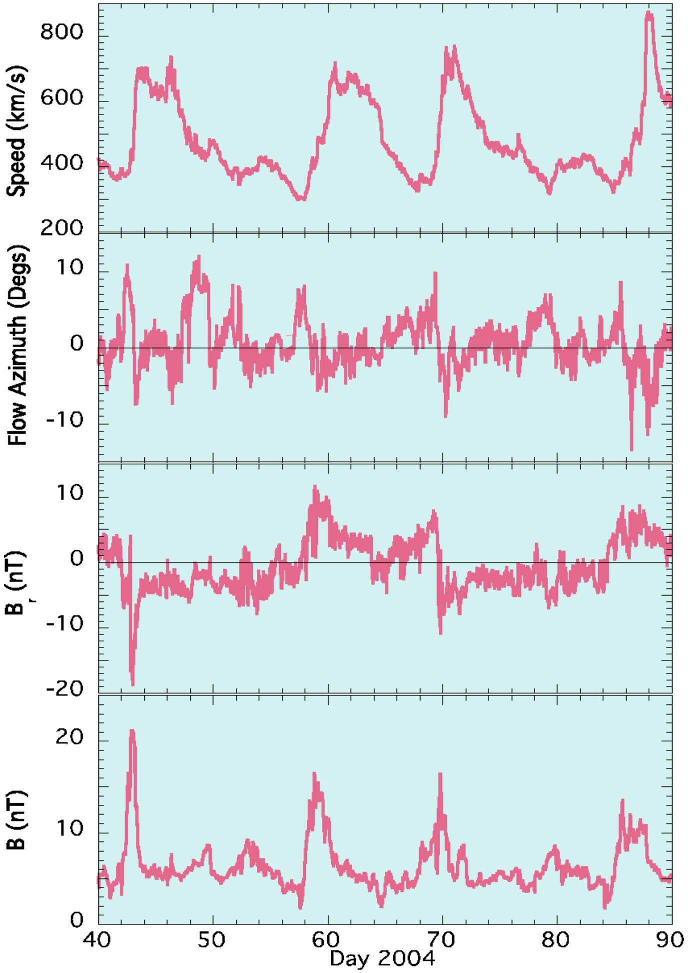

Fig. 1, 2

Purpose

The purpose of this report is to propose a new method for reconstructing the solar wind stream structure beyond Earth’s orbit.

The method is based on the use of two-station interplanetary scintillation data obtained at decameter wavelengths.

Interplanetary scintillations (IPS)

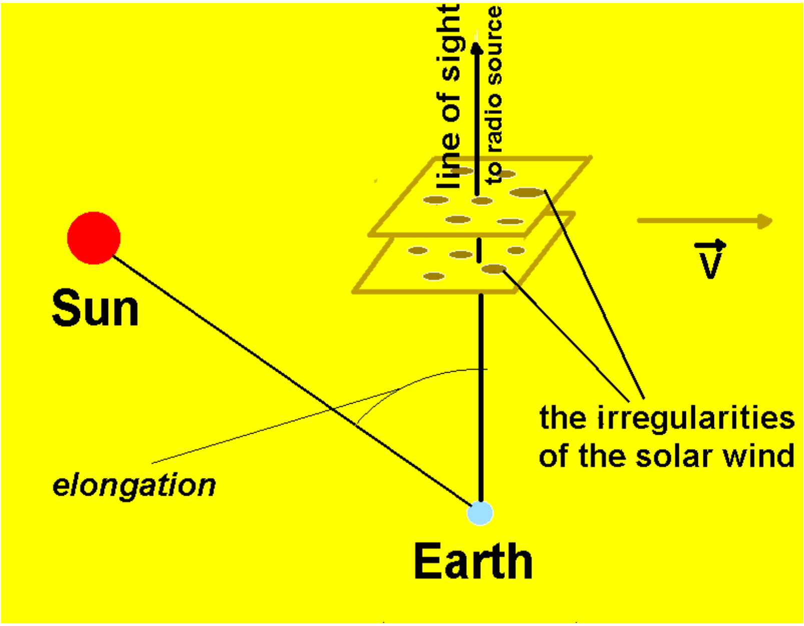

Fig. 3.

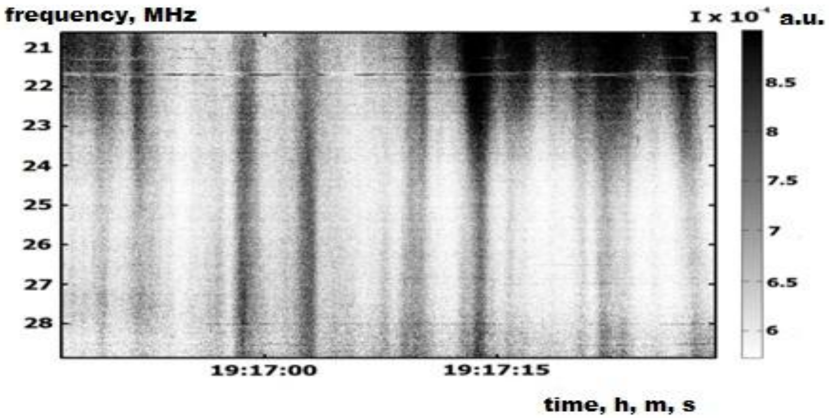

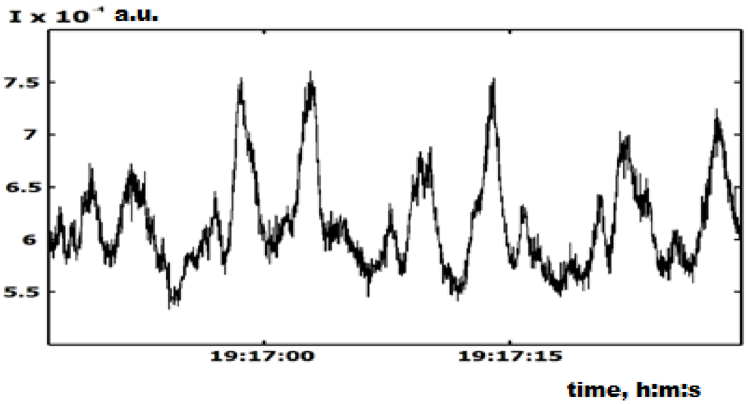

Interplanetary scintillations at decameter wavelengths

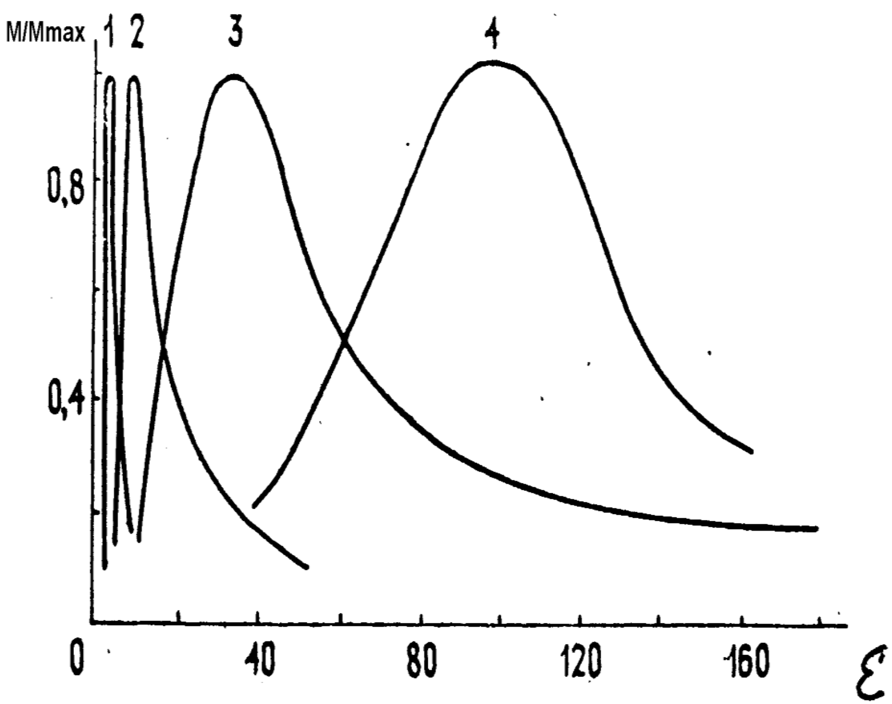

Fig. 4. Dependence of normalized scintillations index m/m_m on solar elongation ε

Where:

m_m - maximum value of scintillations index.

* 1 – 2700 MHz , 3C279;

2 - 430 MHz, CTA-21;

3 - 74 MHz, 3C144;

Erskine F.T., Cronyn W.M., Shawhan S.D., Roelof E.C., Gotwols B.L. Preprint university of Iowa. N77-24. 1977. p.1.

** 4 - 25 MHz, 3C144, UTR-2 .

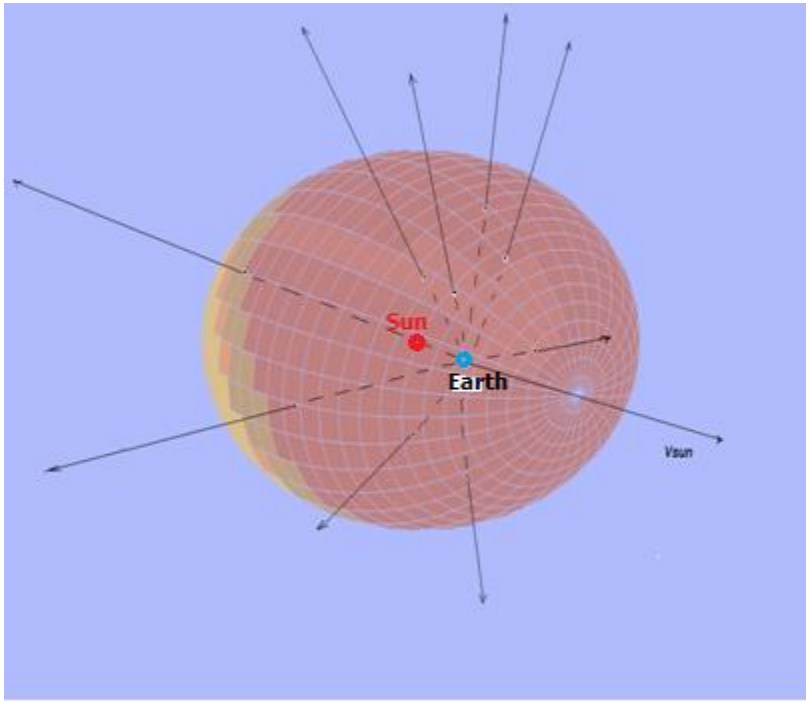

Fig. 5. Decameter range of radio waves provides a real global coverage of the inner heliosphere up to several AU.

Observations. Radio telescopes

UTR-2, 8 – 32 MHz (Kharkiv)

Baseline 152 km oriented east-west

URAN-2, 8 – 32 MHz (Poltava)

Fig. 6.

Harmful effects

- relatively high level of interference, especially at day time
- ionospheric effects

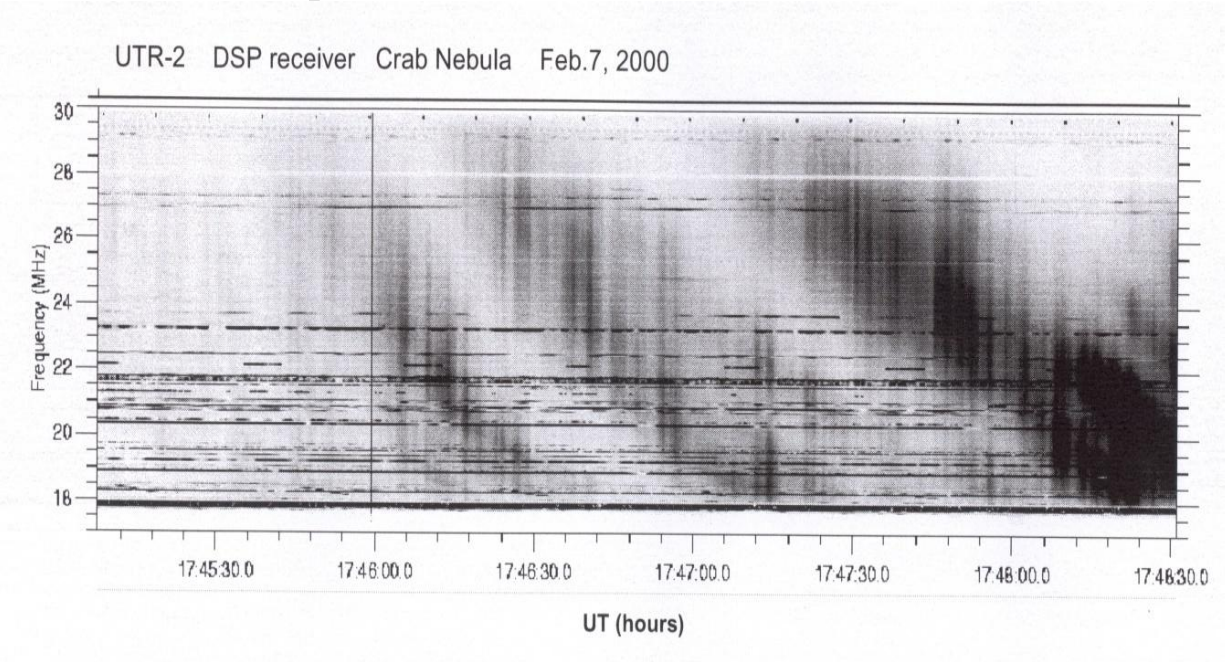

Figure 7. Dynamic spectrum of Crab Nebula scintillations.

We used difference in spatial, temporal and frequency characteristics to separate interplanetary and ionospheric scintillations.

We used digital receivers with high dynamic range that enables us to reject IPS data corrupted by interference.

Synchronous recordings of interplanetary scintillations on two radio telescopes

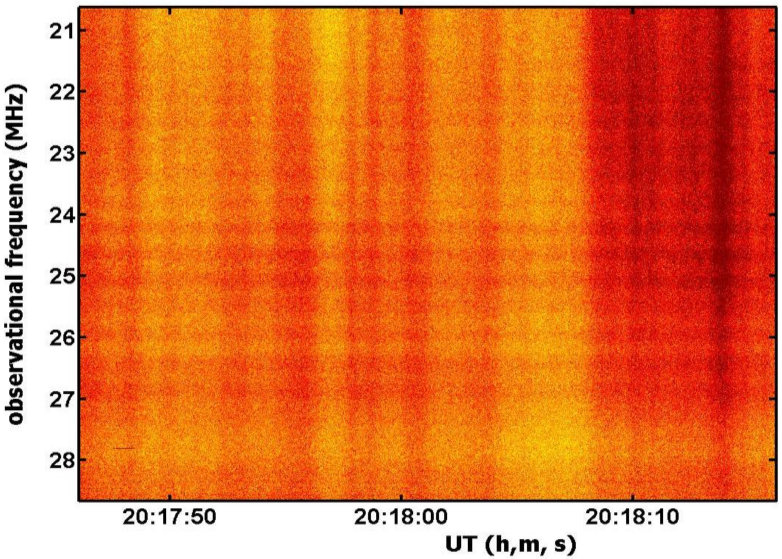

Fig. 8. Dynamic spectrum of interplanetary scintillations of 3C144 (UTR-2)

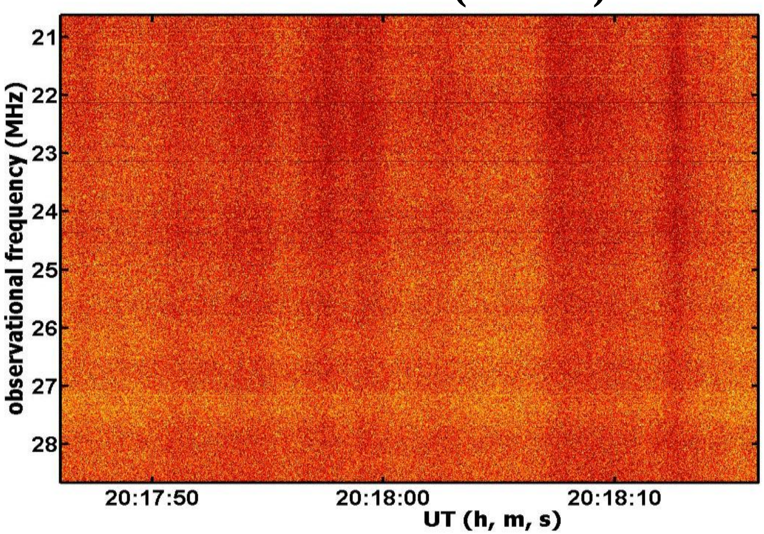

Fig. 9. Dynamic spectrum of interplanetary scintillations of 3C144 (URAN-2)

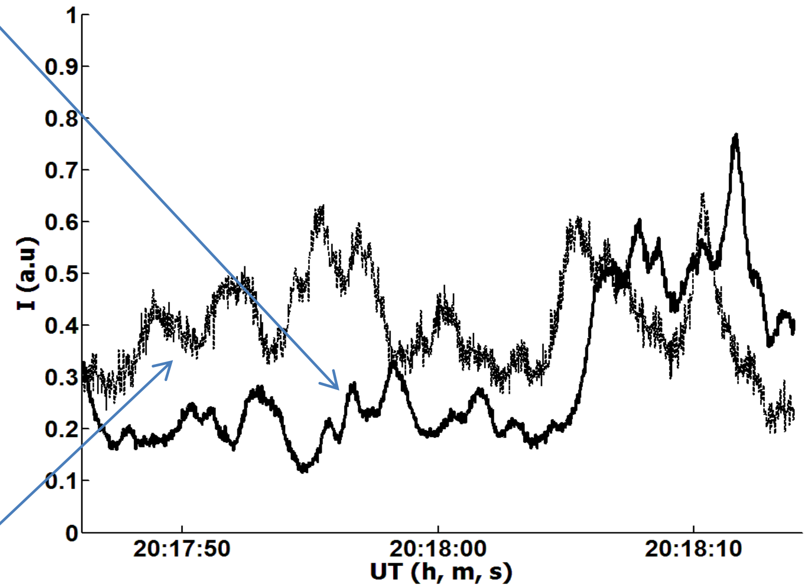

Fig. 10. Cross-sections of dynamic spectra at frequency 25 MHz.

Experimental IPS data processing

Fig.11. Experimental spectra for one (left) and two (right) stream cases.

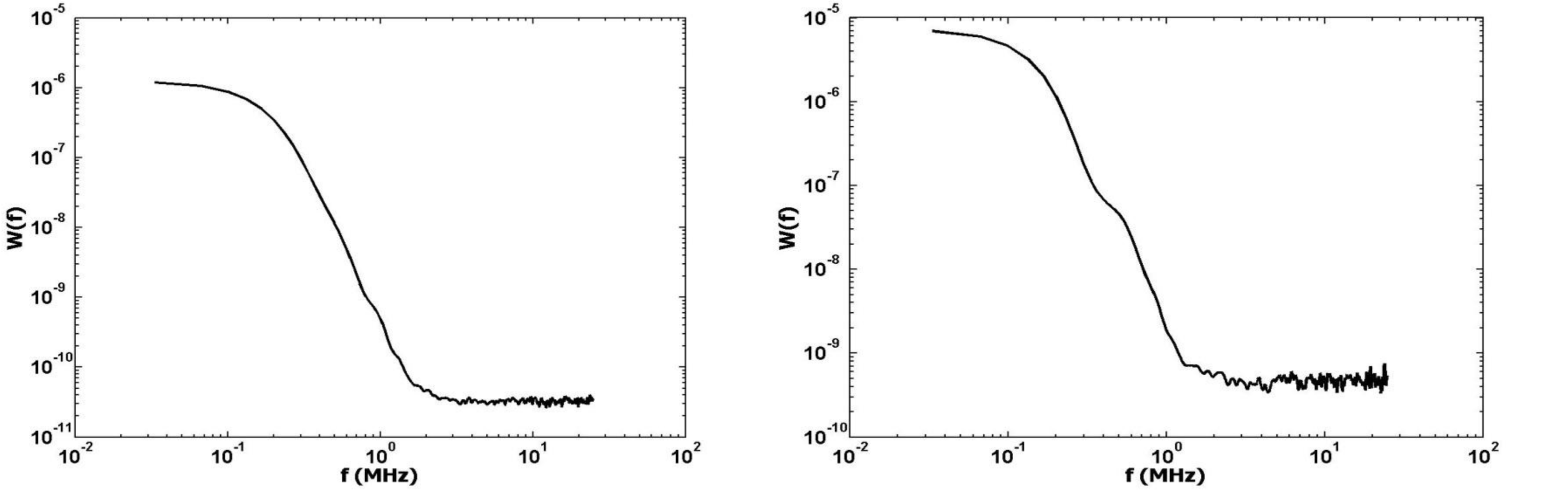

Fig.12. Experimental cross-correlation function for one (solid line) and two (dashed line) stream cases

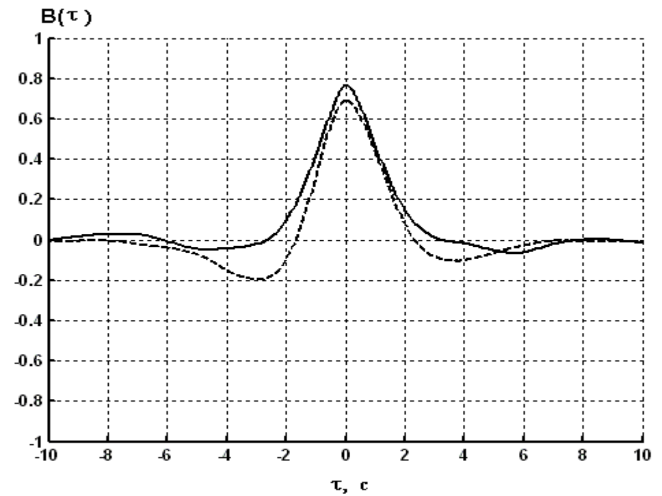

Model fitting

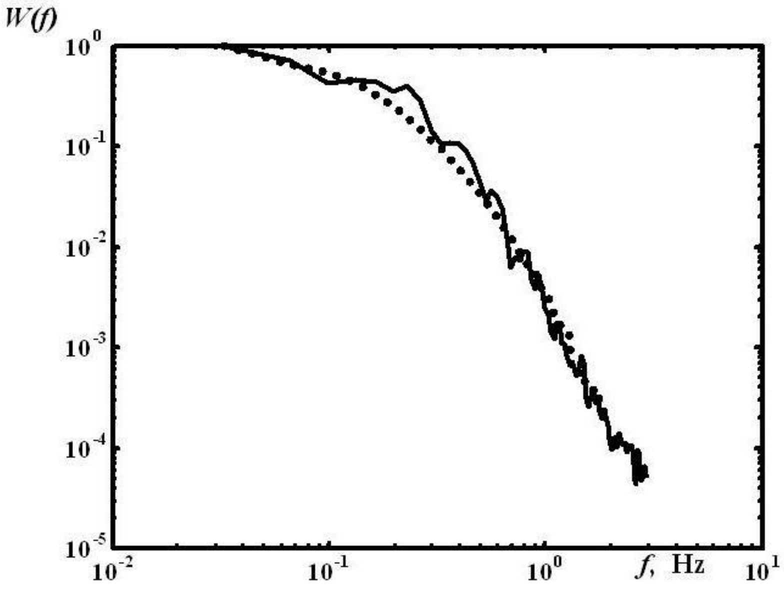

Fig. 13. Scintillation spectrum

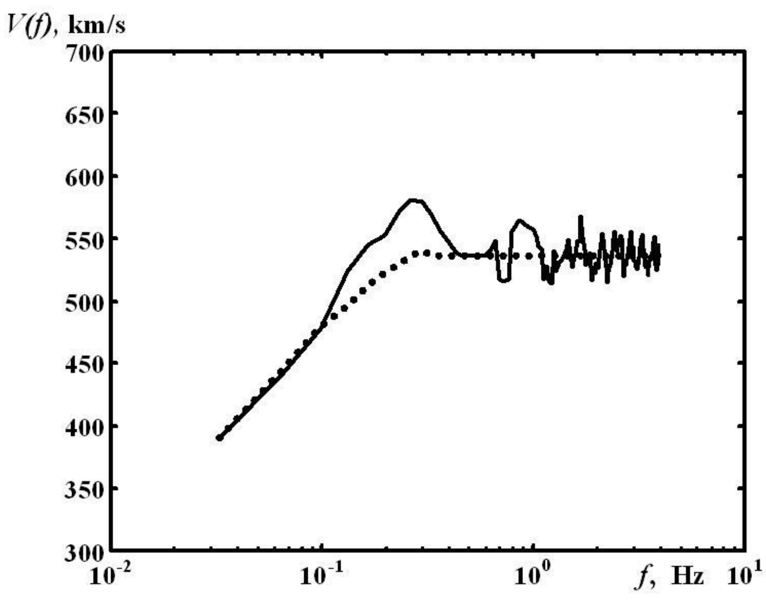

Fig. 14. Velocity of cross spectrum harmonics

$$V_f(f) = 2\pi f b \cos\beta / \Delta\Psi$$

Here $\Delta\Psi = \arccos\left(\mathrm{Re}\,W(b,f)/\left|W(b,f)\right|\right)$

is the phase shift between the antennas for f

-harmonic of cross spectrum $W(b,f)$

Model of the solar wind

m - flows of the solar wind

$v_{1,2,3}$ - velocity

$n_{1,2,3}$ - the spectral index of the interplanetary turbulence spectra

$l_{1,2,3}$ - thickness

Theoretical characteristics

Analysis of scintillation spectrum $W(f)$ and cross-spectrum $W(b,f)$

$$W(f)=\sum_{m=1}^{M}W_m(v_m,f), \qquad (1)$$

$$W_m(v_m,f)\approx 2\pi I_0^2 l_m\left(\frac{4\pi r_e^2}{k}\right)^2\int_0^1 d\zeta\int_{2\pi f/v_{m\perp}(\zeta)}^{\infty}\sin^2\left(\frac{\kappa_{m\perp}^2 l_m\zeta}{2k}\right)\frac{\kappa_{m\perp}\Phi_{Nm}(\kappa_{m\perp},0,\zeta)}{\sqrt{\zeta\left(\kappa_{m\perp}^2 v_{m\perp}^2(\zeta)-4\pi^2 f^2\right)}}\exp\left(-\frac{1}{2}\kappa_{m\perp}^2 L^2\zeta^2\theta_0^2\right)d\kappa_{m\perp},$$

$$W(b,f)=\sum_{m=1}^{M}W_m(b,v_m,f), \qquad (2)$$

$$W_m(b,v_m,f)\approx 2\pi I_0^2 l_m\left(\frac{4\pi r_e^2}{k}\right)^2\int_0^1 d\zeta\int_{2\pi f/v_{m\perp}(\zeta)}^{\infty}\sin^2\left(\frac{\kappa_{m\perp}^2 l_m\zeta}{2k}\right)\exp\left(\frac{2\pi i f b\cos\beta_m}{v_{m\perp}(\zeta)}\right)\frac{\kappa_{m\perp}\Phi_{Nm}(\kappa_{m\perp},0,\zeta)}{\sqrt{\zeta\left(\kappa_{m\perp}^2 v_{m\perp}^2(\zeta)-4\pi^2 f^2\right)}}\exp\left(-\frac{1}{2}\kappa_{m\perp}^2 L^2\zeta^2\theta_0^2\right)d\kappa_{m\perp}.$$

Here $W_m(v_m,f)$ and $W_m(b,v_m,f)$ were caused by scattering inhomogeneities in the m-th flow,

Reconstruction of solar wind structure

12-01-2016
v=540 км/с, n=3.8, l=0.7 a. u.

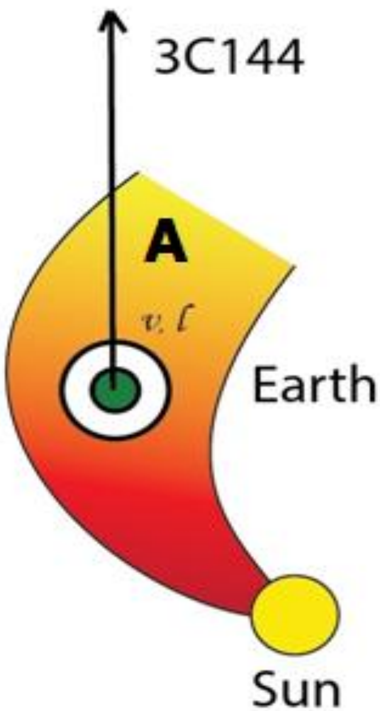

13-01-2016
v_1=530 км/с, n_1=3.9,
l_1=0.4 а.е.,
v_2=400 км/с, n_2=3.9,
l_2=2 а.е.

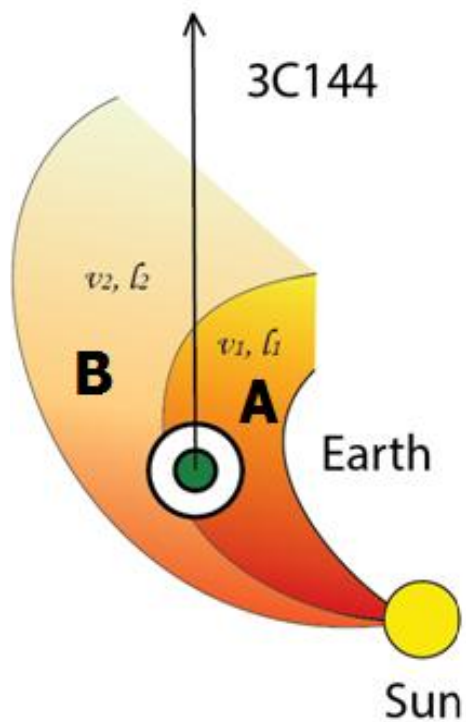

14-01-2016
v_1=400 км/с, n_1=3.8,
l_1=0.2 а.е.,
v_2=540 км/с, n_2=3.7,
l_2=0.3 а.е.,
v_3=480 км/с, n_3=3.8,
l_2=0.5 а.е.

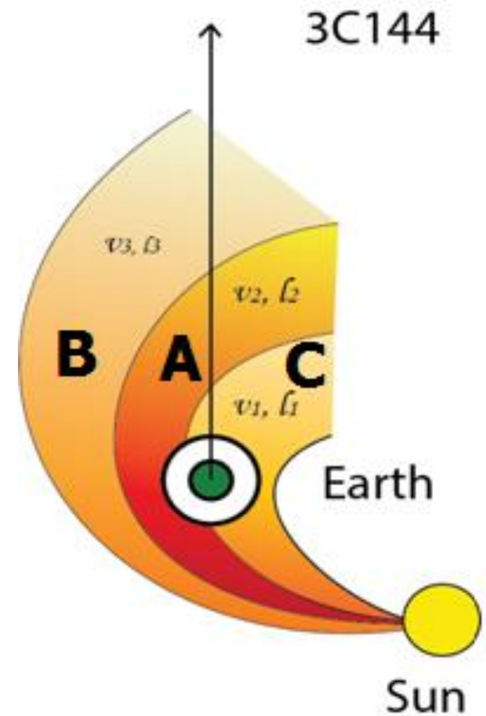

Reconstruction of solar wind structure

15-01-2016
v_1=450 км/с, n_1=3.9,
l_1=0.4 а.е.
v_2=560 км/с, n_2=3.8,
l_2=0.6 а.е.
v_3=290 км/с, n_3=3.8,

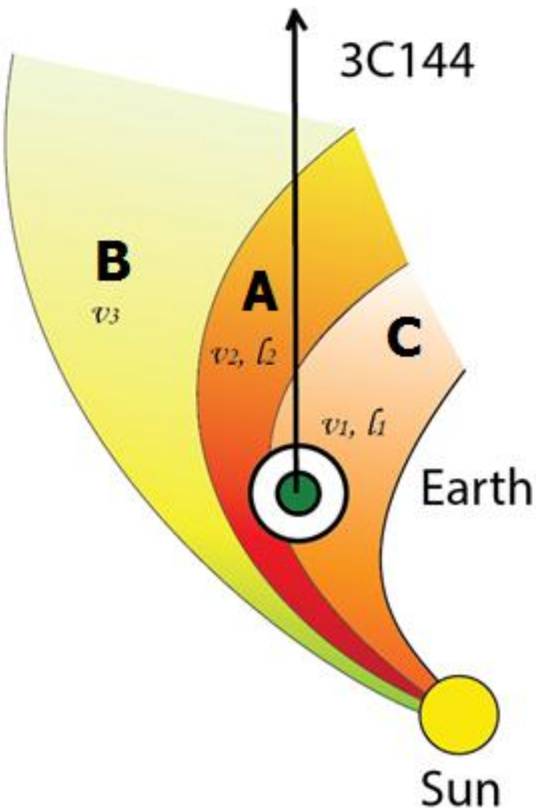

16-01-2016
v_1=280 км/с, n_1=3.7,
l_1=0.3 а.е.
v_2=400 км/с, n_2=3.7,
$l_2 \geq 1.0$ а.е.

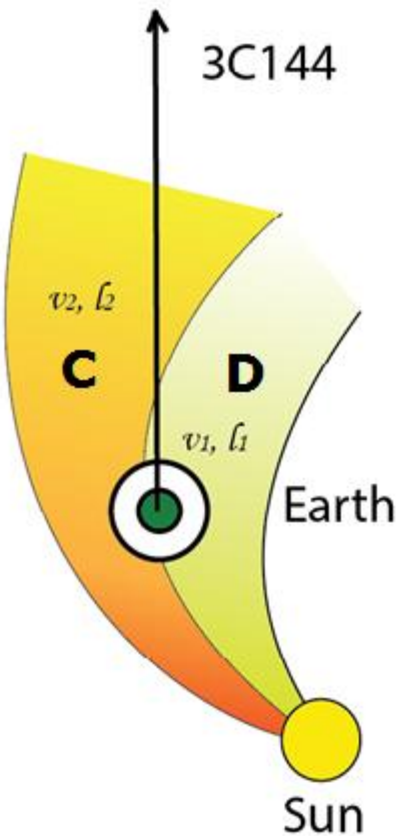

17-01-2016
v_1=260 км/с, n_1=3.7,
a_1=2.7, l_1=0.2 а.е.
v_2=230 км/с, n_2=3.9,
a_2=2.5, l_2=0.2 а.е.
v_3=300 км/с, n_3=3.7,
a_3=2.8, l_2=2.0 а.е.

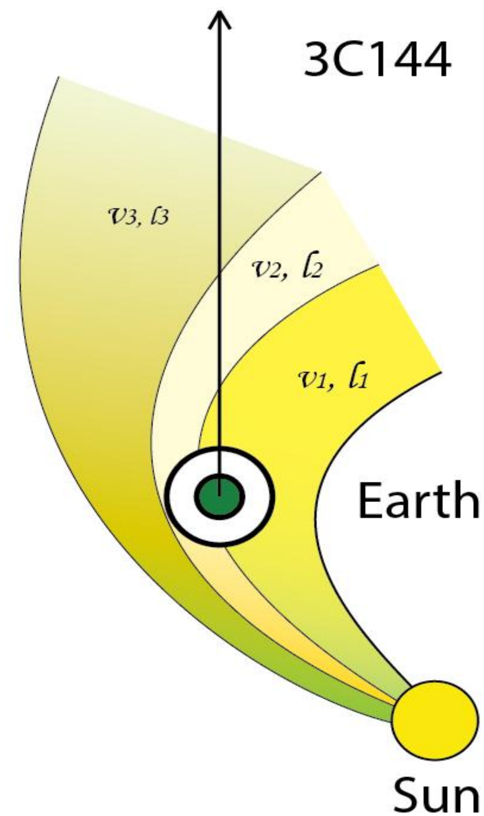

OMNI spacecraft measurements

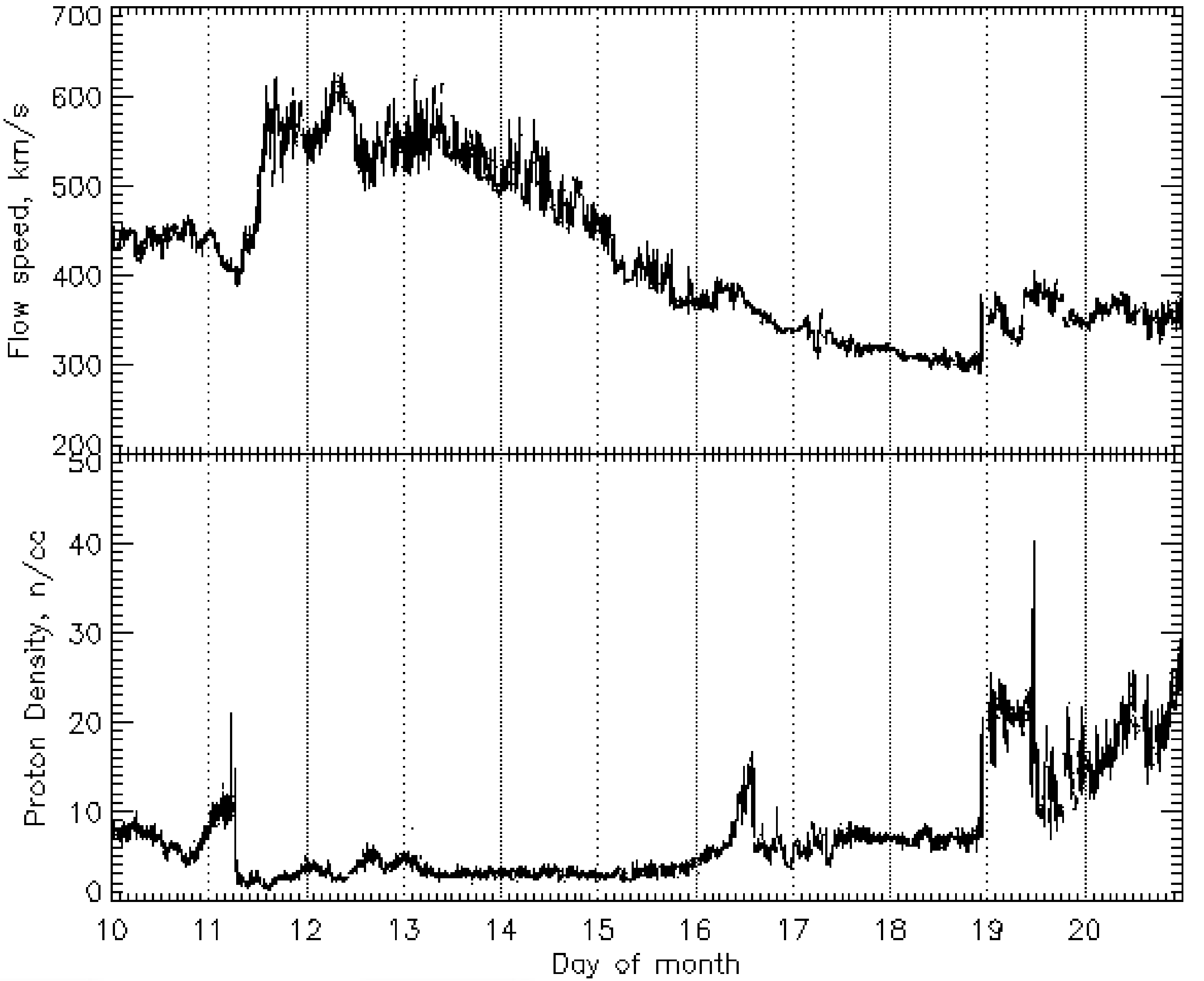

Conclusions and plans for the future

IPS observations at decameter wavelengths allow us to obtain the solar wind parameters and to reconstruct the stream structure of the solar wind.

Future plans

- the use of more scintillating radio sources,

- the use of more IPS characteristics.

Thanks for attention